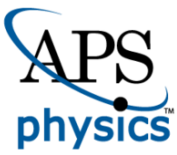

Visualizing ferroic domains in an all-in–all-out antiferromagnet thin film

Y. Kozuka, T. C. Fujita, M. Uchida, T. Nojima, A. Tsukazaki, J. Matsuno, T. Arima, and M. Kawasaki

Phys. Rev. B **96**, 224417 — Published 13 December 2017

DOI: 10.1103/PhysRevB.96.224417

Visualizing ferroic domains in an all-in-all-out antiferromagnet thin film

Y. Kozuka,[1]* T. C. Fujita,[1] M. Uchida,[1] T. Nojima,[2] A. Tsukazaki,[2] J. Matsuno,[3] T. Arima,[3,4] M. Kawasaki[1,3]

[1]*Department of Applied Physics and Quantum Phase Electronics Center, University of Tokyo, 113-8656 Tokyo, Japan.*

[2]*Institute for Materials Research, Tohoku University, Sendai 980-8577, Japan.*

[3]*RIKEN Center for Emergent Matter Science (CEMS), Wako 351-0198, Japan.*

[4]*Department of Advanced Materials Science, University of Toyo, Kashiwa 277-8561, Japan.*

Abstract

Antiferromagnetic domain distribution is analyzed by a scanning superconducting quantum interference device microscopy for a pyrochlore $Tb_2Ir_2O_7$ thin film with all-in-all-out (AIAO) spin arrangement. The local magnetic field on the surface is found to originate predominantly from Tb^{3+} (J = 6) magnetic moment. While Ir^{4+} magnetic moment (J_{eff} = 1/2) is too small to detect even below the Néel temperature (120 K), Tb^{3+} AIAO domains grow below 40 K following the background Ir^{4+} domains rather than the external magnetic field, clarifying the decisive role of Ir-Tb exchange interaction in magnetic ordering.

*corresponding author e-mail: kozuka@ap.t.u-tokyo.ac.jp

I. INTRODUCTION

The interplay between electron correlation (U) and spin-orbit interaction (λ) has attracted much attention in recent years to explore new quantum phases in condensed matters beyond topological insulators [1–4]. The representative materials systems to investigate the spin-orbital Mott physics are 5*d* transition-metal compounds such as iridates [5–21] and osmates [22–25]. Unlike weakly correlated topological insulator, many of the parent compounds inherently exhibit magnetic transitions, which substantially influence the electronic structures [9,15,17–20]. For example, in the case of pyrochlore iridates ($R_2Ir_2O_7$, R: rare-earth ion), which is the target material in this study, a metal-insulator transition is concomitant with an antiferromagnetic transition [5,6], where a variety of topological and nontopological quantum phases have been predicted to emerge below the antiferromagnetic transition temperature (T_N) with U being an adjustable parameter [19–22].

Of particular interest in pyrochlore iridates is the magnetic structure originating from spin frustration. In the pyrochlore crystal structure, rare-earth and Ir sites respectively form corner-sharing tetrahedral network, causing spin frustration in the presence of antiferromagnetic interaction within each sublattice. Given the strong spin-orbit interaction, the ground-state spin structure is theoretically predicted to be antiferromagnetic all-in-all-out (AIAO) structure, where all the four spins at the vertices of the tetrahedra point inward and outward alternatingly as shown in Fig. 1(a) [28]. The AIAO spin ordering has been verified

by a number of experimental studies mainly employing neutron and resonant x-ray diffractions [7,8,15,16,27]. The characteristic feature of AIAO is that, while net dipole moment is zero in the cubic symmetry, this magnetic ordering is regarded as octupole ferroic order with clearly distinctive two magnetic domains [29], which we refer A domain and B domain throughout for simplicity.

Beyond the fascinating electronic and magnetic phases in bulk, distinctive electronic states have been proposed in thin films [30–32] and at the boundaries between A domain and B domain [33,34]. Experimentally, metallic conductivity has recently been found in bulk pyrochlore iridates while the interior of the domains remained a Mott insulator [9,10,12]. These phases at the domain walls could be also accessed in a more controllable way by fabricating artificial A/B domain heterosturctures [35]. Although fabrication of pyrochlore iridate thin films is highly challenging due to high volatility of IrO_3 and low formation energy of tetravalent iridates [36], single-crystalline pyrochlore iridate thin films have recently been synthesized utilizing a solid phase epitaxy based on thermal equilibrium consideration [35,37,38]. Having the pyrochlore iridate thin films, we have demonstrated the domain stabilization and switching based on transport properties [35,37]. However, direct measurements of magnetic domains and correspondence with transport properties have not been reported.

Here, we employ a scanning superconducting quantum interference device (SQUID)

microscopy to visualize the AIAO magnetic domains of a $Tb_2Ir_2O_7$ film [Fig. 1(b)]. Scanning SQUID has been utilized to detect weak and spatially inhomogeneous magnetic field on the surface of samples such as superconductors with vortices [39,40], magnetic oxides [41–44], and magnetically doped topological insulator [45]. Since the magnetic dipole is only induced by the subtle imbalance in antiferromagnetism along [111] anisotropy, scanning SQUID may be one of the most suitable techniques to investigate the magnetization of pyrochlore iridate thin films. In order to perform the scanning SQUID measurement after various field application histories, we have installed a NdFeB permanent magnet which can be inserted on and retracted from the samples. As a result, we clearly visualized the spatial distribution of A and B domains of the Tb^{3+} magnetic moment. Although Ir^{4+} magnetic moment was not directly detected due to the extremely small net magnetization, we found that the Ir^{4+} domains are transcribed to Tb^{3+} domains via Ir-Tb exchange coupling. Finally, we confirm that A or B domains can be selectively stabilized by field cooling. This result confirms that field cooling is an effective way to control AIAO magnetic domains in pyrochlore iridate thin films towards realizing unexplored quantum phases in thin films and heterostructures.

II. EXPERIMENTAL

The details of sample fabrication are explained in Ref. [37]. Briefly, the $Tb_2Ir_2O_7$ thin film was grown by pulsed laser deposition with a KrF excimer laser using a ceramic target made by a hot-press method from a mixture of Tb_4O_7 and IrO_2 powder with a molar

ratio of 1:12 (corresponding to Tb:Ir = 1:3). The film was grown on Y-stabilized ZrO_2 (YSZ) (111) substrate at 450 °C under 100 mTorr O_2 environment with a laser energy of 400 mJ (corresponding to 6 J/cm^2) and a repetition rate of 10 Hz. The lattice mismatch between YSZ ($2a$ = 10.24 Å) and $Tb_2Ir_2O_7$ (a = 10.21 Å) is about 0.3% according to the bulk lattice constants. The structure of the films was characterized by x-ray diffraction, which indicates a (111)-oriented $Tb_2Ir_2O_7$ film is epitaxially grown. The reciprocal space mapping indicates that the out-of-plane lattice is elongated by ~ 0.1% along [111], while the in-plane lattice is shortened by ~ 0.7%. The in-plane lattice contraction is opposite to what is expected from epitaxial strain, and is probably due to distortion caused by nonstoichiometry. The thickness of the $Tb_2Ir_2O_7$ thin film investigated in this study was 100 nm.

We used a commercial scanning SQUID microscope (Seiko Instruments, Inc. SQM2000). The diameter of the pick-up coil is 10 μm, which limits the resolution of the measurement. We installed a NdFeB permanent magnet (5 mm × 5 mm × 2 mm), which can be inserted and retracted to the scanning SQUID chamber by a linear motion feedthrough. The NdFeB magnet was placed right above the sample when the pick-up coil was fully retracted from the sample surface. The polarity of the magnet is also inverted by rotating the feedthrough. The magnet produces about 0.1 T magnetic field at the sample surface. The scanning SQUID images were measured with a scan step of 1.25μm both along x and y axes, which was driven by a stepping motor of the sample stage. The distance between the pick-up

coil and the sample surface is estimated as 1 – 2 μm. Both the sample and the SQUID were cooled with liquid He. We confirmed that the sample can be heated up to 50 K while keeping the SQUID below 3 K for operation.

III. TRANSPORT AND MAGNETIC PROPERTIES

Prior to the scanning SQUID measurement, macroscopic transport and magnetization measurements were carried out. As shown in Fig. 1(c), the resistance shows insulating behavior in all the investigated temperature range with a kink around 120 K (T_N). This kink is considered to be concomitant with the AIAO antiferromagnetic transition of Ir^{4+} spins [5], which is also supported by the present scanning SQUID measurement as discussed later. In our film, increase in the resistivity below T_N is not as steep as that of the bulk with a slightly reduced value of T_N by ~ 10% as well [5]. This is probably due to partial nonstoichiometry of Ir^{4+} in the order of a few percent as studied for bulk $Eu_2Ir_2O_7$ [6]. Another origin of the modest insulating behavior could be distortion from cubic structure acting as external pressure as inferred from the case of $Eu_2Ir_2O_7$ [46]. Figure 1(d) shows temperature dependence of magnetization measured by a SQUID magnetometer under a magnetic field of 0.2 T. The magnetization curve does not exhibit a clear signature of the magnetic transition at T_N, while small bifurcation between field-cooling (FC) and zero field-cooling (ZFC) is discernable. The same behavior has been observed in polycrystalline bulk $Tb_2Ir_2O_7$ and interpreted as induced Tb^{3+} dipole moment via interaction with Ir^{4+}

moment [5, 13]. In contrast to Ir^{4+} spin ordering at T_N = 120 K, the Tb^{3+} moments start to grow below 40 K (T_{Tb}) as indicated by crossing of magnetization between ZFC and FC. Below T_{Tb}, magnetization of FC at +0.2 T (−0.2 T) becomes smaller (larger) than that of ZFC, which indicates that Tb^{3+} moment favor the B (A) domain under positive (negative) FC while the domain of Ir^{4+} sublattice cannot be uniquely determined in this experiment. The AIAO magnetic domains are switchable only at a high magnetic field of ~ 6 T at 2 K as evidenced by hysteresis in the magnetoresistance as shown in Fig. 1(e) as reported for bulk $Nd_2Ir_2O_7$ [11,17]. For the scanning SQUID measurement, we used a magnetic field of ~ 0.1 T in the cooling process, and therefore the AIAO domain switching is ignored throughout.

IV. SCANNING SQUID MICROSCOPY

Having the basic transport and magnetic properties characterized, we show the result of scanning SQUID measurement in Fig. 2. Random magnetic domains with ~ 10 μm scale are clearly visible in the scanning SQUID images. Although net magnetization should be zero in the pyrochlore lattice with cubic symmetry, the clear observation of the magnetic domain structure in the scanning SQUID indicates that the $Tb_2Ir_2O_7$ thin film has finite [111] anisotropy, producing small dipole moment along out-of-plane direction. The origin of the [111] anisotropy may be due to trigonal crystal field braeking cubic symmetry as reported for bulk $Y_2Ir_2O_7$ and $Eu_2Ir_2O_7$ crystals [47,48]. Since the trigonal [111] anisotropy induces opposite dipole moment between A and B domains of AIAO octupole ordering, the domains

with positive and negative magnetization are attributed to respective AIAO domains.

While both Ir^{4+} and Tb^{3+} magnetic moment could contribute to the magnetization, the signal of scanning SQUID is found to be dominated by Tb^{3+} moment. This is verified by measuring the temperature dependence of scanning SQUID images as shown in Figs. 2(a)–2(f). We find that the magnetic field signal rapidly decreases with increasing temperature, and the domains become almost invisible above 40 K as shown in Figs. 2(e) and 2(f). This temperature scale is consistent with T_{Tb} deduced from macroscopic magnetization shown in Fig. 1(d). The root mean square of the magnetic field shows almost the same temperature dependence as neutron scattering intensity of Tb^{3+} for the bulk samples reported in [13], which is also shown in Fig. 2(g). This result indicates the dominant contribution of Tb^{3+} moment in the scanning SQUID over Ir^{4+} moment, consistent with the smaller magnetic moment of Ir^{4+} ($J_{\mathrm{eff}} = 1/2$) than that of Tb^{3+} ($J = 6$).

Irrespective of the visibility by scanning SQUID, the Ir^{4+} spins strongly influence the ordering of Tb^{3+} spins through Ir-Tb exchange interaction. The effect of the Ir-Tb exchange interaction is clearly seen in the FC experiment. Figure 3(a) shows the scanning SQUID image after ZFC, which is basically the same as that in Fig. 2A but in another cooling cycle. After the measurement of ZFC [Fig. 3(a)], the sample is heated to 50 K and subsequently cooled to 4.7 K under a magnetic field of ~ -0.1 T (the permanent magnet is placed just above the sample). The scanning SQUID image after this cooling process is shown in Fig.

3(b), where the domain pattern is almost intact compared with that shown in Fig. 3(a). This result is at first sight quite unexpected, since Tb^{3+} spins almost lose their order around 40 K and might have been biased by the external magnetic field. Instead, the Tb^{3+} domains are almost unchanged even after FC. The recovery of magnetic domains indicates that ordered Ir^{4+} spins keep their domain structures at 50 K ($< T_N$), though invisible by scanning SQUID, and cast the domain structures of Tb^{3+} spins through strong Ir-Tb exchange interaction.

In contrast, significant change in the domain pattern is expected when the sample is heated above T_N (~120 K), where Ir^{4+} spins also lose their order. Figure 3(c) shows a scanning SQUID image measured at 4.7 K after FC from 130 K under a positive magnetic field. In this figure, domain pattern completely changes compared with Figs. 3(a) and (b), indicating that the underlying Ir^{4+} domain structures are also changed. The magnetic field shown in Fig. 3(c) is largely negative across the sample compared with the cases of ZFC [Fig. 3(a)] and FC from 50 K [Fig. 3(b)], which is consistent with smaller magnetization under positive magnetic field cooling in Fig. 1(d). These results visually demonstrate the strong Ir-Tb exchange coupling, determining the pattern of the AIAO domains of Tb^{3+} moment.

V. DISCUSSIONS

Now we discuss the field cooling response of the local magnetization pattern presented above in comparison with macroscopic transport properties. The AIAO domain stabilization by field cooling has been discussed for $Eu_2Ir_2O_7$ thin films based on

magnetotransport in the previous report [37]. There, unconventional linear component in the magnetoresistance was observed after field cooling. As the sign of the linear component was reversed depending on the polarity of the cooling field, the linear magnetoresistance was attributed to selective stabilization of A domain or B domain. In the present study, this assumption can be directly assessed by comparing the linear component of low-field magnetoresistance ($|B| < 3$ T) with magnetization signal obtained by scanning SQUID. Figure 4(a) shows examples of magnetoresistance after field cooling from 130 K with ±0.2T. As in the case of $Eu_2Ir_2O_7$ thin films, magnetoresistance contains an unusual linear component in addition to a standard even component. The α value, defined as the linear component of magnetoresistance ratio per magnetic field, is plotted as a function of cooling magnetic field in Fig. 4(b). The sign of the α value is inverted about zero magnetic field and saturates around $B = \pm 0.05$ T. Given the cooling magnetic field for saturation of α, the scanning SQUID images in Fig. 3(c) is measured for nominally homogeneous B domain. The apparent spatial nonuniformity of magnetization pattern in Fig. 3(c) is probably due to a local variation of [111] anisotropy of the thin film. Nevertheless, our result strongly supports the assumption of selective field-cooling stabilization of the AIAO domains [37].

So far, the AIAO ordering has been measured only macroscopically except one report which visualized AIAO domains of a $Cd_2Os_2O_7$ bulk single crystal by using spatially resolved x-ray magnetic circular dichroism (XMCD) [27]. In the present study, the local

magnetic field pattern directly reflects the spatial distribution of the AIAO antiferromagnetic domains of Tb^{3+} spins. Although XMCD directly probes AIAO domains of Ir^{4+} spins, we have demonstrated that scanning SQUID can be a complementary method to detect the magnetic moment of the rare-earth site.

Finally, we also note that our result is the first successful application of scanning SQUID for antiferromagnetic domains, whereas scanning SQUID have been used to detect local ferromagnetic or superparamagnetic domains of various kinds of magnetic materials [40-45]. In these previous studies, magnetization showed clear hysteresis around zero magnetic field, indicating the presence of spontaneous magnetization. In contrast, our $Tb_2Ir_2O_7$ thin film exhibits negligible remnant magnetization around zero magnetic field as a typical feature of antiferromagnetism. Our study indicates a way to visualize octupole magnetic domains when extrinsic effects such as moderate strain induce dipole moment with breaking cubic symmetry.

After submitting this manuscript, we noticed a recent publication about a neutron study on a bulk $Tb_2Ir_2O_7$ polycrystal, which reveals that deflection of Tb^{3+} moments away from [111] direction below 10 K [49]. This mechanism may generate global magnetization in all-in-all-out spin structure, possibly adding some amount of signal to the scanning SQUID data in this study.

ACKNOWLEDGMENTS

We thank Y. Motome, Y. Kato, M. Nakamura, and Y. Tokura for their valuable comments. This work was performed under the Inter-university Cooperative Research Program of the Institute for Materials Research, Tohoku University (Proposal No.15K0063).

This work was supported by Grant-in-Aids for Scientific Research (S) Nos. 24226002 and 24224010, Challenging Exploratory Research 16K13682 (Y.K.), JSPS Research Fellow No. 26 ·10112 (T.C.F.), Scientific Research on Innovative Areas "Topological Materials Science" No. JP16H00980 (M.U.), and Scientific Research (B) No. 17H02791 (J.M.) from MEXT, Japan, and JST CREST Grant No. JPMJCR16F1, as well as by Asahi-Glass Foundation (Y.K.).

References

[1] D. Pesin and L. Balents, Nat. Phys. **6**, 376 (2010).

[2] M. Kargarian, J. Wen, and G. A. Fiete, Phys. Rev. B **83**, 165112 (2011).

[3] W. Witczak-Krempa, G. Chen, Y. B. Kim, and L. Balents, Annu. Rev. Condens. Matter Phys. **5**, 57–82 (2014).

[4] R. Schaffer, E. Kin-Ho Lee, B.-J. Yang, and Y. B. Kim, Rep. Prog. Phys. **79**, 094504 (2016).

[5] K. Matsuhira, M. Wakeshima, Y. Hinatsu, and S. Takagi, J. Phys. Soc. Jpn. **80**, 094701 (2011).

[6] J. J. Ishikawa, E. C. T. O'Farrell, and S. Nakatsuji, Phys. Rev. B **85**, 245109 (2012).

[7] K. Tomiyasu, K. Matsuhira, K. Iwasa, M. Watahiki, S. Takagi, M. Wakeshima, Y. Hinatsu, M. Yokoyama, K. Ohoyama, and K. Yamada, J. Phys. Soc. Jpn. **81**, 034709 (2012).

[8] H. Sagayama, D. Uematsu, T. Arima, K. Sugimoto, J. J. Ishikawa, E. O'Farrell and S. Nakatsuji, Phys. Rev. B **87**, 100403(R) (2013).

[9] K. Ueda, J. Fujioka, Y. Takahashi, T. Suzuki, S. Ishiwata, Y. Taguchi, M. Kawasaki, and Y. Tokura, Phys. Rev. B **89**, 075127 (2014).

[10] K. Ueda, J. Fujioka, C. Terakura, and Y. Tokura, Phys. Rev. B **92**, 121110(R) (2015).

[11] K. Ueda, J. Fujioka, B.-J. Yang, J. Shiogai, A. Tsukazaki, S. Nakamura, S. Awaji, N. Nagaosa, and Y. Tokura, Phys. Rev. Lett. **115**, 056402 (2015).

[12] E. Y. Ma, Y.-T. Cui, K. Ueda, S. Tang, K. Chen, N. Tamura, P. M. Wu, J. Fujioka, Y. Tokura, and Z.-X. Shen, Science **350**, 538 (2015).

[13] E. Lefrançois, V. Simonet, T. Ballou, E. Lhotel, A. Hadj-Azzem, S. Kodjikian, P. Lejay, P. Manuel, D. Khalyavin, and L. C. Chapon, Phys. Rev. Lett. **114**, 247202 (2015).

[14] T. Kondo, M. Nakayama, R. Chen, J. J. Ishikawa, E.-G. Moon, T. Yamamoto, Y. Ota, W. Malaeb, H. Kanai, Y. Nakashima, Y. Ishida, R. Yoshida, H. Yamamoto, M. Matsunami, S. Kimura, N. Inami, K. Ono, H. Kumigashira, S. Nakatsuji, L. Balents, and S. Shin, Nat. Commun. **6**, 10042 (2015).

[15] H. Guo, C. Ritter, and A. C. Komarek, Phys. Rev. B **94**, 161102 (R) (2016).

[16] C. Donnerer, M. C. Rahn, M. Moretti Sala, J. G. Vale, D. Pincini, J. Strempfer, M. Krisch, D. Prabhakaran, A. T. Boothroyd, and D. F. McMorrow, Phys. Rev. Lett. **117**, 037201 (2016).

[17] Z. Tian, Y. Kohama, T. Tomita, H. Ishizuka, T. H. Hsieh, J. J. Ishikawa, K. Kindo, L. Balents, and S. Nakatsuji, Nat. Phys. **12**, 134 (2016).

[18] M. Nakayama, T. kondo, Z. Tian, J. J. Ishikawa, M. Halim, C. Bareille, W. Malaeb, K. Kuroda, T. Tomita, S. Ideta, K. Tanaka, M. Matsunami, S. Kimura, N. Inami, K. Ono, H. Kumigashira, L. Balents, S. Nakatsuji, and S. Shin, Phys. Rev. Lett. **117**, 056403 (2016).

[19] X. Wan, A. M. Turner, A. Vishwanath, and S. Y. Savrasov, Phys. Rev. B **83**, 205101 (2011).

[20] W. Witczak-Krempa and Y. B. Kim, Phys. Rev. B **85**, 045124 (2012).

[21] W. Witczak-Krempa, A. Go, and Y. B. Kim, Phys. Rev. B **87**, 155101 (2013).

[22] H. Shinaoka, S. Hoshino, M. Troyer, and P. Werner, Phys. Rev. Lett. **115**, 156401 (2015).

[23] T. Bzdušek, A. Riegg, and M. Sigrist, Phys. Rev. B **91**, 165105 (2015).

[24] D. Mandrus, J. R. Thompson, R. Gaal, L. Forro, J. C. Bryan, B. C. Chakoumakos, L. M. Woods, B. C. Sales, R. S. Fishman, and V. Keppens, Phys. Rev. B **63**, 195104 (2001).

[25] J. Yamaura, K. Ohgushi, H. Ohsumi, T. Hasegawa, I. Yamauchi, K. Sugimoto, S. Takeshita, A. Tokuda, M. Takata, M. Udagawa, M. Takigawa, H. Harima, T. Arima, and Z. Hiroi, Phys. Rev. Lett. **108**, 247205 (2012).

[26] S. Calder, J. G. Vale, N. A. Bogdanov, X. Liu, C. Donnerer, M. H. Upton, D. Casa, A. H. Said, M. D. Lumsden, Z. Zhao, J.-Q. Yan, D. Mandrus, S. Nishimoto, J. van den Brink, J. P. Hill, D. F. McMorrow, and A. D. Christianson, Nat. Commun. **7**, 11651 (2016).

[27] S. Tardif, S. Takeshita, H. Ohsumi, J. Yamaura, D. Okuyama, Z. Hiroi, M. Takata, and T. Arima, Phys. Rev. Lett. **114**, 147205 (2015).

[28] M. Elhajal, B. Canals, R. Sunyer, and C. Lacroix, Phys. Rev. B **71**, 094420 (2005).

[29] T. Arima, J. Phys. Soc. Jpn. **82**, 013705 (2013).

[30] B.-J. Yang and N. Nagaosa, Phys. Rev. Lett. **112**, 246402 (2014).

[31] Q. Chen, H.-H. Hung, X. Hu, and G. A. Fiete, Phys. Rev. B **92**, 085145 (2015).

[32] K. Hwang and Y. B. Kim, Sci. Rep. **6**, 30017 (2016).

[33] Y. Yamaji and M. Imada, Phys. Rev. X **4**, 021035 (2014).

[34] Y. Yamaji and M. Imada, Phys. Rev. B **93**, 195146 (2016).

[35] T. C. Fujita, M. Uchida, Y. Kozuka, W. Sano, A. Tsukazaki, T. Arima, and M. Kawasaki, Phys. Rev. B **93**, 064419 (2016).

[36] R. T. Wimber and H. G. Kraus, Metall. Trans. **5**, 1565 (1974).

[37] T. C. Fujita, Y. Kozuka, M. Uchida, A. Tsukazaki, T. Arima, and M. Kawasaki, Sci. Rep. **5**, 9711 (2015).

[38] J. C. Gallagher, B. D. Esser, R. Morrow, S. R. Dunsiger, R. E. A. Williams, P. M. Woodward, D. W. McComb, and F. Y. Yang, Sci. Rep. **6**, 22282 (2016).

[39] C. C. Tsuei and J. R. Kirtley, Phys. Rev. Lett. **85**, 182 (2000).

[40] H. Hilgenkamp, Ariando, H.-J. H. Smllde, D. H. A. Blank, G. Rijnders, H. Rogalla, J. R. Kirtley, and C. C. Tsuei, Nature **422**, 50 (2003).

[41] A. Harada, T. Taniyama, Y. Takeuchi, T. Sato, T. Kyômen, and M. Ito, Phys. Rev. B **75**, 184426 (2007).

[42] J. A. Bert, B. Kalisky, C. Bell, M. kim, Y. Hikita, H. Y. Hwang, and K. A. Moler, Nat. Phys. **7**, 767 (2011).

[43] X. R. Wang, C. J. Li, W. M. Lü, T. R. Paudel, D. P. Leusink, M. Hoek, N. Poccia, A. Vailionis, T. Venkatesan, J. M. D. Coey, E. Y. Tsymbal, Ariando, and H. Hilgenkamp, Science **349**, 716 (2015).

[44] Y. Anahory, L. Embon, C. J. Li, S. Banerjee, A. Meltzer, H. R. Naren, A. Yakovenko, J. Cuppens, Y. Myasoedov, M. L. Rappaport, M. E. Huber, K. Michaeli, T. Venkatesan, Ariando, and E. Zeldov, Nat. Commun. **7**, 12566 (2016).

[45] E. O. Lachman, A. F. Young, A. Richardella, J. Cuppens, H. R. Naren, Y. Anahory, A. Y. Meltzer, A. Kandala, S. Kempinger, Y. Myasoedov, M. E. Huber, N. Samarth, and E. Zeldov, Sci. Adv. **1**, e1500740 (2015).

[46] F. F. Tafti, J. J. Ishikawa, A. McCollam, S. Nakatsuji, and S. R. Julian, Phys. Rev. B **85**, 205104 (2012).

[47] L. Hozoi, H. Gretarsson, J. P. Clancy, B.-G. Jeon, B. Lee, K. H. Kim, V. Yushankhai, P. Fulde, D. Casa, T. Gog, J. Kim, A. H. Said, M. H. Upton, Y.-J. Kim, and J. van den Brink, Phys. Rev. B **89**, 115111 (2014).

[48] D. Uemura, H. Sagayama, T. Arima, J. J. Ishikawa, S. Nakatsuji, H. Takagi, M. Yoshida, J. Mizuki, and K. Ishii, Phys. Rev. B **92**, 094405 (2015).

[49] H. Guo, C. Ritter, and A. C. Komarek, Phys. Rev. B **96**, 144415 (2017).

Figure captions:

FIG. 1. (a) Schematics of (top) Tb and Ir sublattices of $Tb_2Ir_2O_7$ and (bottom) all-in-all-out antiferromagnetic ordering of a Tb^{3+} tetrahedron. (b) Schematic of scanning SQUID measurement for a $Tb_2Ir_2O_7$ thin film grown on a YSZ (111) substrate. The diameter of the pick-up loop is 10 μm. Temperature dependence of (c) resisitivity and (d) magnetization of the $Tb_2Ir_2O_7$ thin film. The magnetization is measured after ZFC and FC with ±0.2 T with increasing temperature under a field strength of +0.2 T applied along [111]. (e) Magnetic field dependence of resistivity at 2 K.

FIG. 2. (a–f) Scanning SQUID images at different temperatures after ZFC. The size of the images is 60 μm × 60 μm. (g) Temperature dependence of the root mean square of magnetic field for the scanning SQUID images. The scaled neutron intensity from Tb^{3+} magnetic moment is also shown for comparison, which is taken from Ref. [13].

FIG. 3. Scanning SQUID images of (a) ZFC, (b) FC from 50K, and (c) FC (+0.1 T) from 130 K. A negative magnetic field is applied when field cooling for (b), while it is positive for (c). The measurement temperature is 4.7 K for all the data. The magnetic field is applied in the cooling processes with a NdFeB permanent magnet placed just above the sample.

FIG. 4. (a) Magnetoresistance at 2 K after the sample is cooled from 130 K under ±0.2 T. The α value is defined as linear component of magnetoresistance per magnetic field. (b) The α value as a function of cooling magnetic field.

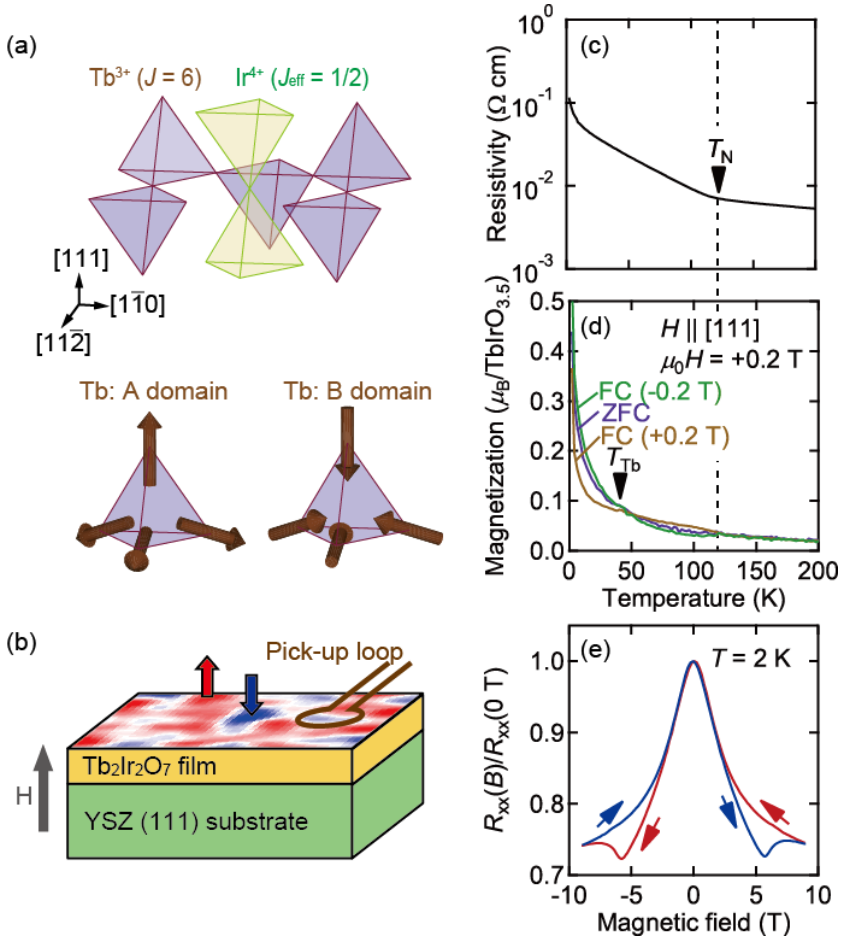

Fig. 1 Y. Kozuka *et al.*

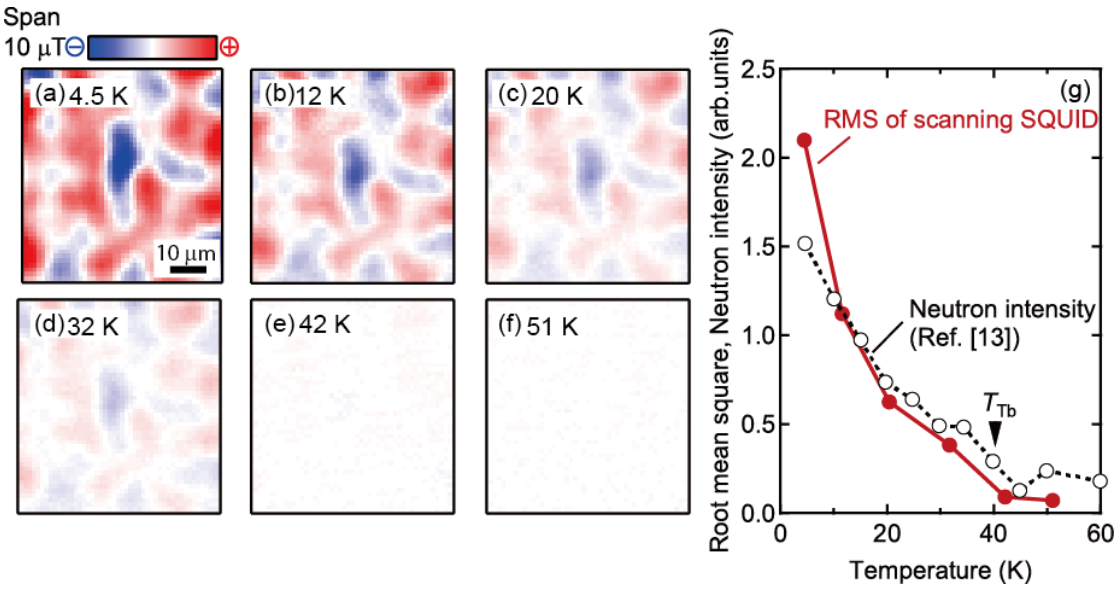

Fig. 2 Y. Kozuka *et al.*

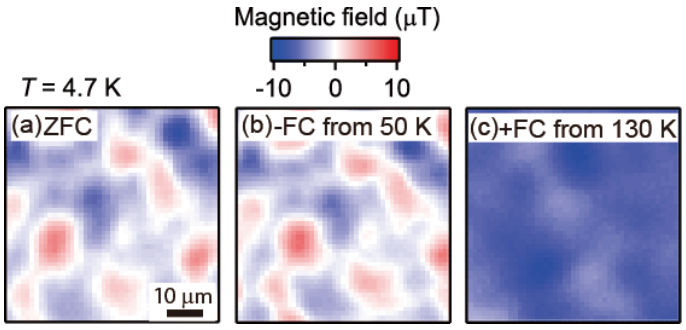

Fig. 3 Y. Kozuka *et al.*

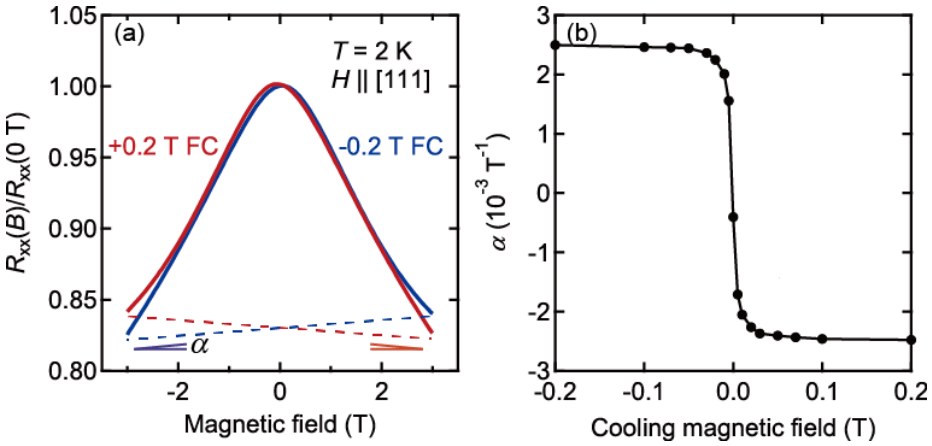

Fig. 4 Y. Kozuka *et al.*